

Derivation of an empirical potential for gold with angular corrections

Stéphane Olivier,* Riccardo Conte, and Alessandro Fortunelli†
 Molecular Modeling Laboratory, IPCF-CNR, Via G. Moruzzi 1, Pisa, I56124, Italy
 (Received 21 July 2007; published 19 February 2008)

From a detailed analysis of density-functional calculations on gold model clusters and surfaces, an empirical potential for gold, which includes angular corrections, is derived. This potential introduces higher-order non-linear terms (specifically, the product dipole-quadrupole) that do not seem to have been previously used, but that are necessary to describe directionality effects in the gold-gold interaction. Preliminary tests show that the proposed empirical potential possesses novel features with respect to the existing ones, such as a strong tendency of small Au clusters toward cage configurations, and represents a good starting point for future investigations.

DOI: 10.1103/PhysRevB.77.054104

PACS number(s): 61.46.Bc, 31.50.Bc, 68.35.B-

I. INTRODUCTION

Several empirical potentials have been proposed and are often successfully used to describe the physics of the metal-metal interaction. Among these, the most popular are the Rosato, Guilloupe, Legrand (RGL),¹ embedded atom model (EAM),² glue-model³⁻⁵ potentials, and their variants. In general, in all these empirical schemes it is assumed that the total energy of the system can be expressed as the sum of site atomic energies with a many-body character, i.e., depending in an analytically compact form upon the number, distance, and orientation of the neighbors of each given metal atom:

$$E^{\text{tot}} = \sum_i^{\text{atoms}} E_i^{\text{atomic}}(\vec{r}_{ij}, j \neq i), \quad (1)$$

where $\vec{r}_{ij} = \vec{r}_j - \vec{r}_i$, with \vec{r}_i, \vec{r}_j the vectors of the coordinates of the atoms i and j . As a norm, the atomic energies E_i^{atomic} are assumed to depend on the coordinates of all the other atoms through generalized collective variables (GCV), i.e., functions which describe the distribution of neighbors around the given atom in a collective way. What distinguishes the various empirical potentials is then the choice of the GCV and the analytic form by which the E_i^{atomic} depend upon the GCV. As an example, the RGL energy expression reads¹

$$E_i^{\text{RGL}} = A \sum_{j \neq i}^{\text{atoms}} \exp \left[-p \left(\frac{r_{ij}}{r_0} - 1 \right) \right] - \xi \left\{ \sum_{j \neq i}^{\text{atoms}} \exp \left[-2q \left(\frac{r_{ij}}{r_0} - 1 \right) \right] \right\}^{1/2}, \quad (2)$$

where A and ξ are positive coefficients, p and q are the exponents of the repulsive and attractive terms, respectively, r_0 is the first-neighbor distance in the bulk (for fcc gold, $r_0 = 2.885 \text{ \AA}$), and r_{ij} is the modulus of \vec{r}_{ij} . The glue-model energy expression similarly reads³⁻⁵

$$E_i^{\text{glue-model}} = \sum_{j \neq i}^{\text{atoms}} V(r_{ij}) - F \left[\sum_{j \neq i}^{\text{atoms}} n(r_{ij}) \right], \quad (3)$$

where $V(r)$, $F(x)$, and $n(r)$ are functions often (but not necessarily) described as a set of points that are connected by cubic splines. Many empirical energy expressions (such as

EAM and RGL) are just particular cases of the general glue-model expression. However, the GCV in Eq. (3) only depend on the moduli of the interatomic distances r_{ij} . Baskes^{6,7} was the first to call for the introduction of angular terms into the potential, i.e., terms depending on the angular distribution of neighbors around a given atom. The form he proposed is based on the theory of the multipolar expansion of the density defined as a set of points. The lowest-order terms of this expansion are the dipole, the quadrupole and the octupole, whose analytic forms read

$$\text{dipole} = \sum_{\sigma=x,y,z} \left[\sum_{j \neq i}^{\text{atoms}} \rho^{\text{dipole}}(r_{ij}) \frac{r_{ij}^{\sigma}}{r_{ij}} \right]^2, \quad (4)$$

$$\text{quadrupole} = \sum_{\sigma=x,y,z} \sum_{\sigma'=x,y,z} \left[\sum_{j \neq i}^{\text{atoms}} \rho^{\text{quadrupole}}(r_{ij}) \frac{r_{ij}^{\sigma} r_{ij}^{\sigma'}}{r_{ij}^2} \right]^2 - \frac{1}{3} \left[\sum_{j \neq i}^{\text{atoms}} \rho^{\text{quadrupole}}(r_{ij}) \right]^2, \quad (5)$$

$$\text{octupole} = \sum_{\sigma=x,y,z} \sum_{\sigma'=x,y,z} \sum_{\sigma''=x,y,z} \left[\sum_{j \neq i}^{\text{atoms}} \rho^{\text{octupole}}(r_{ij}) \frac{r_{ij}^{\sigma} r_{ij}^{\sigma'} r_{ij}^{\sigma''}}{r_{ij}^3} \right]^2 - \frac{3}{5} \sum_{\sigma=x,y,z} \left[\sum_{j \neq i}^{\text{atoms}} \rho^{\text{octupole}}(r_{ij}) \frac{r_{ij}^{\sigma}}{r_{ij}} \right]^2, \quad (6)$$

where $\rho^k(r)$ are functions of r , and the corresponding energy contributions are functions of these expressions. In Eqs. (4)–(6), the $\rho^k(r)$ functions can be given a simple exponential form⁶⁻⁹ or described as a set of points that are connected by cubic splines in the spirit of glue models.¹⁰ The corresponding modified EAM (MEAM) or modified glue models have proven to often give improved results with respect to the original spherical models.^{7,10,11} It is worthwhile noting that there is often a cancellation of terms in Eq. (6), such that the octupole assumes appreciable values only when the dipole is zero. In general, it should be also recalled that these contributions are identically null for cubic systems (fcc, bcc, simple cubic).

The case of gold is particularly interesting in this context: it has been shown in fact that directionality effects are im-

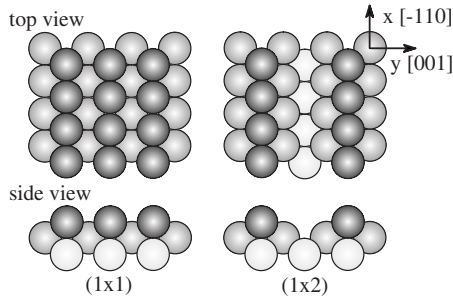


FIG. 1. Schematic representation of the Au(110) surface and its missing-row reconstruction.

portant in determining the structure and energetics of gold nanoclusters.^{12–16} These effects can only be described within an empirical potential formalism through angular-dependent terms. Given the scientific and technological importance of gold clusters and surfaces it is therefore of great interest to search for an empirical potential which can describe directionality effects in the gold-gold interaction. This would open the way to a more realistic simulation of systems such as catalytically active supported gold clusters, organic monolayers self-assembled on gold surfaces, etc. There already exist empirical potentials which include angular corrections for gold. However, preliminary tests using two different MEAM potentials, the one proposed in Ref. 7 and one derived according to the protocol described in Ref. 17, have shown that the existing potentials do not improve in a qualitatively significant way with respect to the standard RGL or EAM approaches in the description of directionality effects in gold systems. Tight-binding approaches have also been proposed¹⁸ but their results are also not fully satisfactory.

In this work, we pursue the derivation of a gold-gold empirical potential which includes angular-dependent terms. Through a detailed analysis of the energetics of model systems, we show that the reasons of the failure of existing empirical potentials to account for the peculiar directionality effects of Au-Au interactions are to be found in the lack of higher-order nonlinear terms (such as the product dipole-quadrupole). We include one such a term in our fit, thus deriving a new Au-Au potential with unusual characteristics, and producing results more in line with what is currently known about the structure and relaxation of gold clusters and surfaces.

In our analysis, we will often refer to a particular gold surface: the missing-row reconstructed Au(110) surface. Experimentally, a missing row reconstruction has been observed on the Au(110) surface with several techniques such as low energy electron spectroscopy,^{19–23} field ion microscopy,^{24–26} ion scattering,^{27–32} x-ray diffraction,³³ electronic microscopy,³⁴ and scanning tunneling microscopy.³⁵ The fcc (110) surface and its (1×2) reconstruction are shown in Fig. 1. This anisotropic surface orientation can be described with two inequivalent unit vectors along the $[\bar{1}10]$ and the $[001]$ directions (which we call, respectively, x and y). The atom density in the x direction is higher than in the y direction (the interatomic distances are, respectively, $a/\sqrt{2}$ and a , with a the fcc lattice parameter). The missing row reconstruction consists in removing one every two dense rows (see Figs. 1

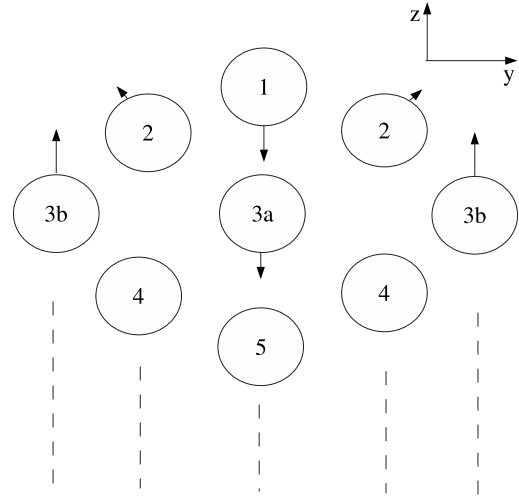


FIG. 2. Schematic picture (side-view) of the Au (110) missing-row reconstructed surface. The atoms explicitly shown are those selected in our simplified “surface-only” Au (110) system. The orientation of coordinates in the (y,z) plane is also shown. The arrows indicate the directions of the final reconstruction according to DF calculations.

and 2), leading to a succession of (111) microfacets. Its interest in this context lies in its peculiar structural relaxation (experimentally observed and essentially in agreement with first-principles calculations) such that the (111) microfacets tend to assume a concave rather than a convex habitus.³⁶ This is shown in a pictorial way in Fig. 2: the atoms lying on the (111) microfacets, labeled as atom-2 in Fig. 2, tend to move slightly outwards, instead of inwards, and is put on a quantitative basis in Table I, where the structural parameters of the reconstructed and fully relaxed Au(110) surface are reported. This “rounding” of low-index faces in gold clusters and surfaces has been previously observed^{14–16} and indicated as a signature of directionality or angular-dependent effects. As an example, in Table II the geometrical parameters for the Au₃₈ truncated octahedral cluster are reported, as obtained from first-principles calculations, whence it is apparent that the atoms lying on the (111) faces tend to expand and protrude out of the surface plane.

II. COMPUTATIONAL DETAILS

Density-functional (DF) calculations are performed using the PWSCF (plane-wave self-consistent field) computational code,³⁷ and employing ultrasoft pseudopotentials to describe the interaction between the outer-shell electrons with the inner shell electrons and the nucleus. The PW91 exchange-correlation functional,³⁸ which is a gradient-corrected functional, is employed. The kinetic energy cutoff for the selection of the plane-wave basis set is set at 544 eV for all the calculations. A procedure of Gaussian broadening of the one-electron energy levels is applied (with a value of 0.68 eV as the smearing parameter). The k -point sampling of the Brillouin zone is changed according to the conductive properties of the systems. In the case of extended systems, which are conductive (small energy gap between HOMO and

TABLE I. Values of the differences in geometrical parameters with respect to the bulk structure for the complete fcc (110) surface (including 15 layers) or its simplified “surface-only” version, optimized through various empirical potential (RGL, POT) and first-principles (LDA, PW91) approaches. POT is the potential derived in the present work. The parameters for the RGL potential were taken from Ref. 1. LDA is the local-density exchange-correlation functional. PW91 is the Perdew-Wang exchange-correlation functional (Ref. 38). All values are in Å.

	Δz_1	Δz_2	Δz_{3a}	Δz_{3b}	Δy_2
complete (110) surface					
LDA	-0.229	0.028	-0.114	0.168	0.026
PW91	-0.335	0.014	-0.202	0.161	0.011
RGL	-0.199	-0.040	-0.042	0.065	-0.041
POT	-0.248	0.024	-0.163	0.319	0.027
simplified “surface-only” (110) surface					
PW91	-0.090	0.030	0	0	0.040
RGL	-0.196	-0.048	0	0	-0.004
POT	-0.197	0.002	0	0	0.046

LUMO), twelve k points are used in each extended direction. For finite systems (Au_{38} and Au_6 clusters), only the Gamma point is used. The geometry optimizations are stopped when maximum force on atoms are less than 0.005 eV/\AA . The dimension of the unit cell is chosen so as to leave a distance of at least $6\text{--}8 \text{ \AA}$ between atoms on neighboring cells for finite systems. The PW91 results are reported after rescaling the energies by a factor 1.18794 and the distances by a factor 0.9786, so as to reproduce the experimental binding energy per atom of 3.83 eV and equilibrium first-neighbor distance of 2.885 \AA for fcc gold. Note that the (110) surface is relaxed by fixing the lattice constant to the DF-relaxed value, not to the experimental value, and finally rescaled by the 0.9786 factor. The DF description of the energetics of gold systems is known to depend sometimes appreciably upon the choice of the exchange-correlation functional, the pseudopotential, and the numerical approach used for the solution of the DF equations.^{16,39–42} In this context, the PW91 functional appears to produce results which are in reasonable agreement with the experimental data. The main qualitative points of the following analysis have anyway been found to hold also with a different choice of the exchange-correlation functional.

TABLE II. Values of the geometrical parameters for the Au_{38} truncated octahedral cluster optimized through various empirical potential (RGL, POT) and first-principles (PW91) approaches. POT is the potential derived in the present work. The parameters for the RGL potential were taken from Ref. 1. PW91 is the Perdew-Wang exchange-correlation functional (Ref. 38). All values are in Å.

	zcore	zvertex	yvertex	zface
RGL	2.006	1.954	3.900	2.067
PW91	1.974	1.993	3.963	2.294
POT	1.937	1.947	3.826	2.377

III. THE APPROACH

The approach we use in the derivation of the gold-gold potential is essentially based on a detailed analysis of the energetics of model systems. As in all empirical schemes, we assume that the total energy of the system can be expressed as the sum of site atomic energies E_i^{atomic} , see Eq. (1), which depend on the coordinates of all the other atoms through generalized collective variables (GCV). A basic GCV quantity which will be used to orient our analysis is the coordination number, i.e., the number of first neighbors, obtained by neglecting all atoms at a distance larger than, say, 15% of the first-neighbor distance in the bulk. Model systems are then chosen in which the coordination number and the internuclear distances span the range encountered in typical physical systems, and the corresponding energy results are carefully analyzed, trying to derive information on the analytic forms aptest to describe the physics of the metal-metal interaction. Our fitting set is thus a set of DF/PW91 energies of model systems in ideal configurations for different values of the first-neighbor internuclear distance. As “ideal configurations” we mean that all first-neighbor distances have the same value, and only an overall “breathing” of the structure is allowed (i.e., a multiplication of all the coordinates by the same factor). This choice allows us to keep the underlying physics under control. Once the physical range of the parameters has been found, a final refinement using a larger fitting set and the force-matching method^{43,44} can be profitably used to improve accuracy. Our aim here is however to achieve a basic understanding of the factors at stake in the gold-gold interaction, trying to avoid that numerics obscure the physics underneath.

The model systems we have selected are as follows.

(1) fcc: the structure of bulk gold, with coordination number=12 and no bonding anisotropy.

(2) The fcc (111) bilayer (111BL), taken as a simplified example of the fcc (111) unreconstructed surface, with coordination number=9 and a strong bonding anisotropy.

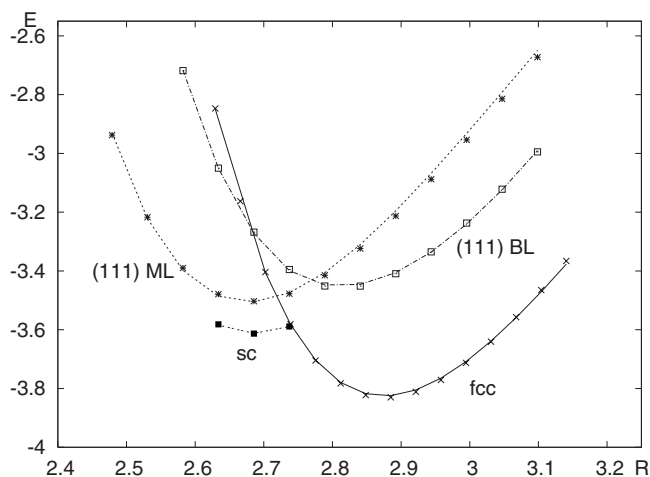


FIG. 3. The DF/PW91 (points) and our atom-atom potential (full-line) energies for several gold systems: fcc (crosses, continuous line); (111) monolayer (asterisks, short-dotted line); (111) bilayer (empty squares, point-dotted line); simple cubic (sc, filled squares, long-dotted line). The energy (in eV) is reported as a function of the first neighbor distance (in Å).

(3) The fcc (111) monolayer (111ML), a configuration which is also rather common (as argued below), with coordination number=6 and a small bonding anisotropy.

(4) The fcc (100) bilayer (100BL), taken as a simplified example of the fcc (100) unreconstructed surface, with coordination number=8 and a strong bonding anisotropy.

(5) The fcc (100) monolayer (100ML), with coordination number=4 and a small bonding anisotropy.

(6) Simple cubic (sc): the simple cubic arrangement, with coordination number=6 and no bonding anisotropy.

(7), (8) 2fcc and 1fcc: two 3D fcc-like structures obtained by taking the fcc four-atom simple cubic supercell and by deleting atoms on (100) faces for 2fcc, or atoms on both (100) and (010) faces for 1fcc, respectively, with coordination numbers=8 (respectively, 4) for 2fcc (respectively, 1fcc) and a small bonding anisotropy, chosen as counterparts of the fcc (100) bilayer and monolayer, respectively.

(9) A simplified “surface-only” fcc (110) surface: the system shown in Fig. 2, with coordination numbers=7 (atom 1), 9 (atom 2), 10 (atom 3b), and 12 (atom 3a), respectively, and a strong bonding anisotropy except for the 3a atoms.

(10) Au₃₈: the Au₃₈ cluster in its truncated octahedral configuration, with coordination numbers=6 for the 24 apex atoms, 9 for the 8 atoms on the fcc (111) faces, and 12 for the 6 core atoms, respectively, and a strong bonding anisotropy except for the core atoms.

(11) Au₆: the Au₆ cluster in its octahedral configuration, with coordination number=4 and a strong bonding anisotropy.

We underline again that these structures are not fully relaxed, but are taken in ideal configurations, with all the first-neighbor distances equal, and are only allowed to “breathe” as a function of the first-neighbor distance. Figures 3–5 show the properly rescaled DF/PW91 energies for the selected model systems which have been used in the fit of the potential.

We start our analysis by justifying our choice of the fcc (111) monolayer as a fitting system. This is a very common

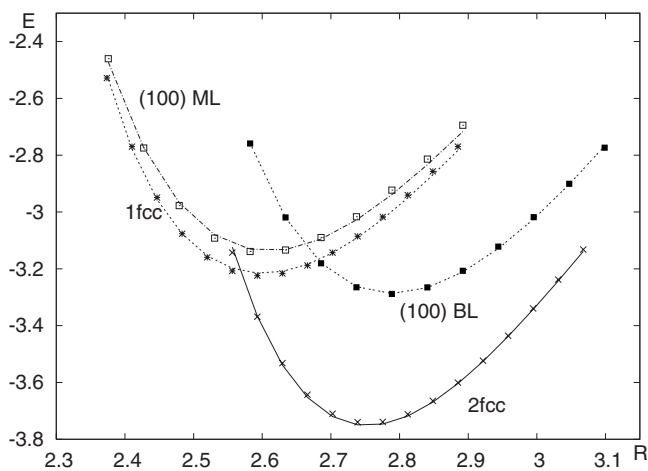


FIG. 4. The DF/PW91 (points) and our atom-atom potential (full-line) energies for several gold systems: (100) monolayer (empty squares, point-dotted line); (100) bilayer (filled squares, long-dotted line); fcc missing atoms on (100) and (010) faces (asterisks, short-dotted line); fcc missing atoms on (100) faces (crosses, continuous line). The energy (in eV) is reported as a function of the first neighbor distance (in Å).

structural motif, typical of many systems, including reconstructed surfaces and clusters. As an example, for the fcc (110) missing-row reconstructed surface, as a result of the appreciable structural relaxation of atoms 3a and 3b, with 3a penetrating deeply into the bulk and 3b moving upward to the surface, atom 2 in practice decreases its coordination number from 9—i.e., the value of an fcc (111) surface—to 6, i.e., the value of an fcc (111) monolayer. Analogously, in the rosettelike amorphization mechanism of the 55-atom icosahedron, described in Ref. 14 for Pt₅₅ but common also to Au₅₅, a bulk atom below the reconstructed icosahedral vertex moves to the surface to form (together with its six first neighbors) what is essentially an fcc (111) monolayer. The reasons

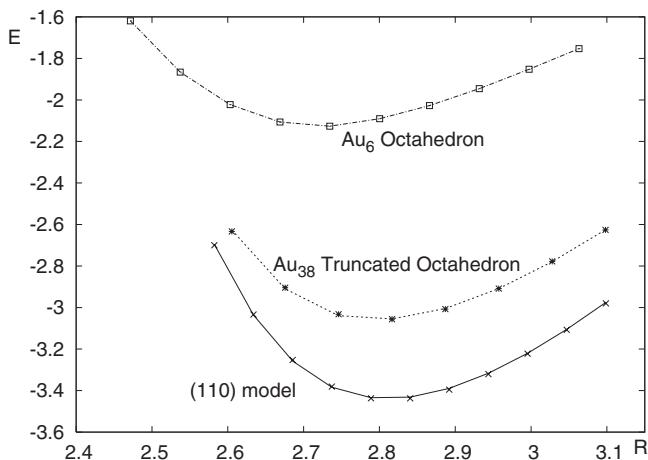


FIG. 5. The DF/PW91 (points) and our atom-atom potential (full-line) energies for several gold systems: simplified “surface-only” (110) system, see Fig. 2 (crosses, continuous line); Au₃₈ truncated octahedron (asterisks, dotted line); Au₆ octahedron (squares, point-dotted line). The energy (in eV) is reported as a function of the first neighbor distance (in Å).

of this ubiquitous presence are apparent from Fig. 3: if only a breathing is allowed, but no relaxation of the interlayer distance, the binding energy per atom of the fcc (111) bilayer (≈ 3.45 eV) is smaller than the binding energy per atom of the fcc (111) monolayer (≈ 3.50 eV). The bilayer is thus formally unstable with respect to dissociation into two monolayers (obviously, when interlayer relaxation is allowed, the bilayer energy drops below the monolayer energy, but only by 0.09 eV). This also explains why angular terms in the potential are necessary for an accurate description of gold-gold bonding: using a spherical coordination number as the only variable would either overestimate the binding energy of the fcc (111) bilayer (underestimate the surface energy), or underestimate the binding energy of the fcc (111) monolayer (i.e., overestimate the stability of compact vs planar configurations). As we will see below, among the angular terms, the dipolar one in particular will be necessary to describe such an effect.

The second point which can be drawn from an inspection of Fig. 3 concerns the weight of the quadrupolar term, through a comparison of the simple cubic and fcc (111) monolayer results. These two systems have the same coordination number, but a different number of second neighbors, and also different angular contributions: The dipolar and octupolar terms are zero by symmetry for both systems, whereas the quadrupolar term is zero for the simple cubic (as for all cubic systems), but nonzero for the fcc (111) monolayer. Indeed, the simple cubic energy lies below the 111ML energy in Fig. 3. However, this difference can be explained essentially in terms of second- and further-neighbor contributions, as confirmed by the fact that by fitting the 111 ML energy curve with an RGL-like expression, and using the RGL parameters so derived to evaluate the simple cubic energy, we found a good agreement with the true simple cubic results. This implies that the quadrupolar contribution is not large, presumably much smaller than the dipolar one, and we thus chose to ignore it altogether. Moreover, we only included three points of the simple cubic curve into our fitting set to give more weight to the fcc (111) monolayer arrangement, which is a much more common configuration. Analogously, we also ignore the octupolar contribution, which—by a similar analysis—we found to be much smaller than the dipolar one.

In passing, we report the result of a test of the assumption that the total energy can be expressed as the sum of site atomic energies: The energies of an fcc (111) trilayer (with three atoms in the unit cell) and the sum of the fcc bulk (with one atom in the unit cell) and the 111 BL (with two atoms in the unit cell) are within 0.02 eV up to a first-neighbor distance of 2.90 Å. This confirms that it is meaningful to analyze these systems in terms of a site-dependent energetics.

IV. PARAMETRIZATION OF THE SPHERICAL MODEL

We start from the parametrization of the spherical component of the potential, i.e., the terms which are nonzero for systems presenting a center of inversion, and thus lacking the dipolar term: fcc, 111 ML, sc, 2fcc, 100 ML, 1fcc. Prelimi-

nary tests showed that an RGL-like analytic form was able to reasonably describe the energy curves of Figs. 3 and 4, but that for improving the accuracy the coefficients of the repulsive and attractive terms should depend on the coordination number of the atoms involved, in a spirit analogous to that at the basis of glue models.³⁻⁵

We thus chose the following analytic form, which is a mixture of the RGL and glue-model energy expressions:

$$E^{\text{tot}} = \sum_i^{\text{atoms}} E_i^{\text{sph}}, \quad (7)$$

$$E_i^{\text{sph}} = A_i \sum_{j \neq i}^{\text{atoms}} \exp \left[-p \left(\frac{r_{ij}}{r_0} - 1 \right) \right] - \xi_i \left\{ \sum_{j \neq i}^{\text{atoms}} \exp \left[-2q \left(\frac{r_{ij}}{r_0} - 1 \right) \right] \right\}^{1/2}, \quad (8)$$

where the first (second) term on the right-hand-side is the usual repulsive (attractive) RGL-like contribution, but the linear coefficients A_i and ξ_i now depend upon effective coordination numbers (or GCV):

$$A_i = A^{(0)} + A^{(1)}c_i + A^{(2)}c_i^2 + A^{(3)}c_i^3, \quad (9)$$

$$\xi_i = \xi^{(0)} + \xi^{(1)}d_i + \xi^{(2)}d_i^2 + \xi^{(3)}d_i^3, \quad (10)$$

where c_i , d_i are GCV, defined as

$$c_i = \sum_{j \neq i}^{\text{atoms}} f(r_{ij}; \alpha_c, R_c), \quad (11)$$

$$d_i = \sum_{j \neq i}^{\text{atoms}} f(r_{ij}; \alpha_d, R_d) \quad (12)$$

with the weight function f defined as

$$f(r; \alpha, R) = \begin{cases} \{1 + \exp[\alpha(r - R)]\}^{-1}, & r \leq R, \\ 0.5 \cdot \exp[-\alpha(r - R)/2], & r \geq R. \end{cases} \quad (13)$$

Note that f is continuous with its derivative at R by construction and that (being a Fermi distribution for $r \leq R$) it “saturates” to 1 for $r \rightarrow 0^+$, while it decays exponentially for $r \rightarrow \infty$. The rationale for this choice of the f function is that saturation for $r \rightarrow 0^+$ prevents the GCV from growing without limit at small distances, while the junction with the exponential function for $r \geq R$ assures a slower decay than the Fermi distribution. We decided not to describe f in terms of general polynomials (as in glue models) to limit the number of nonlinear parameters in the fitting procedure (i.e., only p , q , α_c , α_d , R_c , R_d). We thus minimized Δ , the mean square-root deviation between the empirical potential energies and the DF/PW91 energies, for the spherical model systems. The linear parameters $A^{(0)}$, $A^{(1)}$, $A^{(2)}$, $A^{(3)}$, $\xi^{(0)}$, $\xi^{(1)}$, $\xi^{(2)}$, $\xi^{(3)}$ were obtained through a least-square fit, keeping the nonlinear parameters fixed. The nonlinear parameters were obtained through a basin-hopping global-optimization procedure,^{45,46} which is known to be efficient and cost effective for this kind of problem. The final values of all parameters are reported in

TABLE III. Values of the optimized linear and nonlinear parameters for the spherical model. Radii are in Å.

parameter	value	parameter	value
p	12.40566	q	3.75564
α_c	8.2366	R_c	3.315329
α_d	4.436801	R_d	3.864539
$A^{(0)}$	0.197011	$\xi^{(0)}$	1.496829
$A^{(1)}$	-0.033297	$\xi^{(1)}$	0.026087
$A^{(2)}$	0.003679	$\xi^{(2)}$	-0.002991
$A^{(3)}$	-0.000116	$\xi^{(3)}$	0.0000886

Table III, and correspond to a value of $\Delta=0.0096$ eV (72 points).

V. PARAMETRIZATION OF THE DIPOLAR CONTRIBUTION

The dipolar contribution is by far the most delicate one. This is due to the fact that it is a differential contribution, in which all the inaccuracies of the spherical model are also hidden, and above all to the elusive nature of the directional, orientation-dependent interactions that this term is invoked to deal with.

As a first try, we chose an analytic form for the dipolar contribution along the lines of Eqs. (7) and (8):

$$E = \sum_i^{\text{atoms}} (E_i^{\text{sph}} + E_i^{\text{dip}}), \quad (14)$$

$$E_i^{\text{dip}} = D_i \sum_{\sigma=x,y,z} \left[\sum_{j \neq i}^{\text{atoms}} P(r_{ij}; R_M) \frac{r_{ij}^\sigma}{r_{ij}} \right]^2, \quad (15)$$

where the sum over σ in the right-hand-side is the dipolar term, multiplied by a linear coefficient D_i expressed as a third-order polynomial of an effective coordination number e_i :

$$D_i = D^{(0)} + D^{(1)}e_i + D^{(2)}e_i^2 + D^{(3)}e_i^3 \quad (16)$$

with

$$e_i = \sum_{j \neq i}^{\text{atoms}} f(r_{ij}; \alpha_e, R_e). \quad (17)$$

Moreover, to allow the dipolar contribution the maximum possible freedom (which is necessary, as the detailed energetics of gold clusters via empirical potentials is very sensitive to the choice of the dipolar term), we expressed the $P(r; R_M)$ function in terms of a sixth-order polynomial in $r - R_M$, as usual in glue models

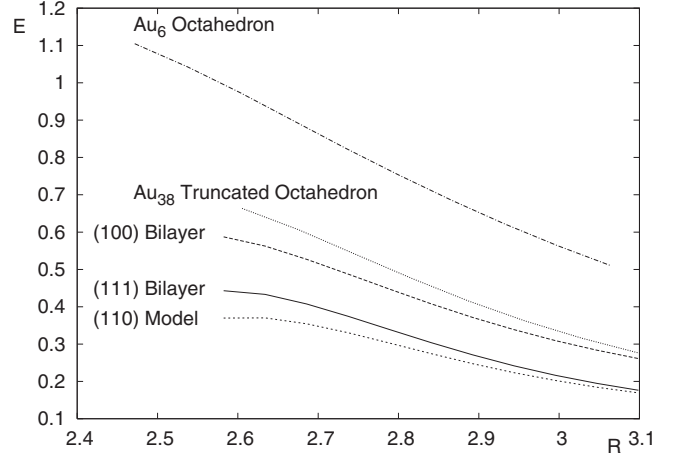


FIG. 6. Plots of the dipolar energy contribution, i.e., the difference between the DF/PW91 binding energy per atom and the spherical component per atom of our atom-atom potential for several gold systems: (111) bilayer (continuous line); (100) bilayer (long-dotted line); simplified “surface-only” (110) system (medium-dotted line); Au_{38} truncated octahedron (short-dotted line); Au_6 octahedron (point-dotted line). Note that the contribution for the (110) system is smaller than for the other surface systems because the energy per atom is considered. Within the dipolar contribution, $E_i^{\text{dip-quad}}$ has a minimum around 3.3 \AA representing roughly -10 – 16 % of the total dipolar contribution for the surface systems, is small (around -1 %) for Au_{38} , and is roughly constant and around $+20$ % for Au_6 . Energies in eV, distances in Å.

$$P(r; R_M) = \begin{cases} p^{(2)}(r - R_M)^2 + p^{(3)}(r - R_M)^3 \\ + p^{(4)}(r - R_M)^4 + p^{(5)}(r - R_M)^5 \\ + p^{(6)}(r - R_M)^6 & \text{if } r \leq R_M, \\ 0 & \text{if } r \geq R_M. \end{cases} \quad (18)$$

Note that $P(r; R_M)$ is continuous with its derivative at R_M . As a technical aside, in glue models $P(r; R_M)$ is often defined in terms of polynomials over splinlike intervals. We found this unnecessary, as the choice of a polynomial over a single interval assures one to reach a comparable accuracy, at the same time reducing the number of nonlinear parameters.

With this choice of the analytic form for the dipolar term we conducted an extensive search (using the basin-hopping algorithm) for the best possible values of the nonlinear parameters, with the linear parameters obtained as before via a least-square fit. The main result of this extensive search was that it is impossible to accurately describe the energetics of the fitting set using only the dipolar term: Major discrepancies between DF and empirical potential results still remained. The reason for this failure is apparent from Fig. 6, where we plot the differences $E_i^{\text{DF/PW91}} - E_i^{\text{sph}}$ for the dipolar systems included in our fitting set. From an inspection of Fig. 6, one can see that (1) the dipolar contribution tends to level off at small r , and most importantly that (2) these differences do not scale even in an approximately linear way with the number of dipolar first-neighbors, calculated by limiting the sum over neighbors in the definition of the dipolar

term in Eq. (15) to first neighbors only, and assuming that they are all at the same distance, which gives a rough estimate of the size of the dipolar contribution. This number reads (for the dipolar systems included in our fitting set): six for 111BL, eight for 100BL, four for octahedral Au₆, nine for atom-1, six for atom-2, one for atom-3b, in the simplified version of the fcc (110) reconstructed surface. This led us to conclude that for an accurate reproduction of the dipolar contribution one needs to introduce a dependence of the coefficients D_i upon the distribution of the neighboring atoms. This represents a higher-order effect, but one that is apparently important. A rough analysis also shows that the square or the cube of the dipole are not appropriate, as a more subtle dependence is at play. The octupole is also excluded, as it is usually too small to produce a sizeable effect. At the same order in the multipolar expansion as the octupole and the cube of the dipole, one finds the product of the dipole by the quadrupole. We thus added to the empirical potential expression a product contribution of the form

$$E_i^{\text{dip-quad}} = DQ_i \text{dipole} \cdot \left\{ \sum_{\sigma=x,y,z} \sum_{\sigma'=x,y,z} \sum_{j \neq i}^{\text{atoms}} \exp \left[-\alpha_q \left(\frac{r_{ij}}{r_0} - 1 \right) \right] \frac{r_{ij}^{\sigma} r_{ij}^{\sigma'}}{r_{ij}^2} \right\}^2 - \frac{1}{3} \left\{ \sum_{j \neq i}^{\text{atoms}} \exp \left[-\alpha_q \left(\frac{r_{ij}}{r_0} - 1 \right) \right] \right\}^2, \quad (19)$$

where dipole is the usual dipolar term defined in Eq. (15) without the D_i factor, and the sum over σ , σ' and $j \neq i$ in the right-hand-side is the quadrupolar term, multiplied by a linear coefficient DQ_i which is expressed as a third-order polynomial in an effective coordination number e_i :

$$DQ_i = DQ^{(0)} + DQ^{(1)}e_i + DQ^{(2)}e_i^2 + DQ^{(3)}e_i^3. \quad (20)$$

Note that to avoid a proliferation of nonlinear parameters, and since the product (dipole times quadrupole) is only a correction term, we used a simple exponential for the radial dependence of the quadrupole, and that the coefficient DQ_i of the product term $E_i^{\text{dip-quad}}$ depends on the same effective coordination number e_i as the coefficient of the “pure” dipolar term.

As before, with this choice of the analytic form for the dipolar term we conducted an extensive search (using the basin-hopping algorithm) for the best possible values of the non-linear parameters, with the linear parameters obtained via a least-square fit. We found that in this case it was possible to obtain an excellent fit of all the energy curves in Figs. 3–5. It can also be noted in passing that—despite the fact that the coefficients of the $P(r;R_M)$ polynomial describing the radial part of the dipolar contribution were left completely unconstrained and only one interval was used in its definition—the resulting behavior, shown in Fig. 7, does not present any nonphysical oscillations, and tends to saturation for small values of the distance. The final optimal parameters for the dipolar term are given in Table IV, and correspond to a value of $\Delta=0.0083$ eV (123 points). The quality of the

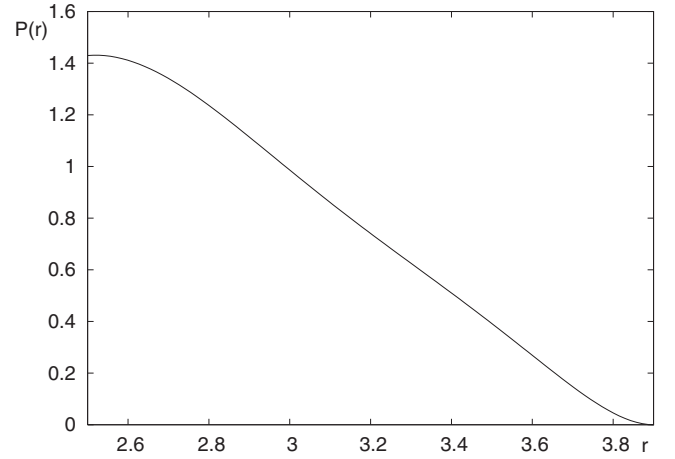


FIG. 7. Plot of $P(r;R_M)$, the polynomial describing the radial component of the dipolar contribution to the energy, as a function of r (in Å), see text for details.

final fit is shown in Figs. 3–5, and in our opinion can be considered as satisfactory, with absolute differences between DF and empirical potential energies of the order of 0.01 eV.

VI. TEST OF THE EMPIRICAL POTENTIAL

The first test of the new potential consisted in evaluating the values of some bulk quantities and comparing them with experimentally derived values and with the results of calculations using our DF approach. This comparison is reported in Table V. From an inspection of this table, it can be seen that the new potential is in reasonable agreement with both experiment and DF results. The tendency to underestimate the stacking fault energy is typical of RGL-like approaches when this quantity is not explicitly introduced into the fitting set, while the overestimation of the vacancy formation energy with respect to DF witnesses an overshooting of the directional contribution at high coordination number which anyway goes in the direction of a better agreement with experiment.

TABLE IV. Values of the optimized linear and nonlinear parameters for the dipolar component. Radii are in Å.

parameter	value	parameter	value
α_e	5.747017	R_e	3.125850
α_q	4.008572	R_M	3.9
$D^{(0)}$	0.115741	$DQ^{(0)}$	0.133939
$D^{(1)}$	-0.035967	$DQ^{(1)}$	-0.061012
$D^{(2)}$	0.00606144	$DQ^{(2)}$	0.0087037
$D^{(3)}$	-0.00034804	$DQ^{(3)}$	-0.00039698
$p^{(2)}$	5.706506		
$p^{(3)}$	12.521950		
$p^{(4)}$	13.436660		
$p^{(5)}$	6.718205		
$p^{(6)}$	1.211088		

TABLE V. Comparison between some experimental bulk quantities (exp.) for gold and the same quantities as predicted by the potential (POT) derived in the present work, or evaluated via our density-functional (DF) approach (properly rescaled as detailed in the text). E_v^F , E_{sf} and the various σ are calculated at $T=0$ and include relaxation effects. σ^{111} , σ^{100} refer to unreconstructed surfaces, σ^{110} refers to the missing-row reconstructed surface.

Quantity	POT	exp.	DF
Lattice parameter a (Å)	4.08	4.08	4.08
Cohesive energy E_c (eV/atom)	3.83	3.83	3.83
Stacking fault energy E_{sf} (mJ/m ²)	5	<55	26
Vacancy formation energy E_v^F (eV)	0.86	0.94	0.55
Bulk Modulus B (10 ¹² dyne cm ⁻²)	1.927	1.803	1.793
C_{11} (10 ¹² dyne cm ⁻²)	2.208	2.016	2.166
C_{12} (10 ¹² dyne cm ⁻²)	1.786	1.697	1.606
C_{44} (10 ¹² dyne cm ⁻²)	0.612	0.454	0.283
Surface energy σ^{111} (meV/Å ⁻²)	58.1	96.8	57.3
Surface energy σ^{110} (meV/Å ⁻²)	69.2	—	68.6
Surface energy σ^{100} (meV/Å ⁻²)	128.2	—	123.0

The second test of the new potential consisted in fully relaxing the model structures which were used as fitting systems from their ideal configurations: the simplified “surface-only” Au(110) surface, the complete Au(110) surface and the Au₃₈ truncated octahedral cluster. The results of such calculations are reported in Tables I and II. An inspection of these tables immediately shows that the present potential improves upon the description of the missing-row Au(110) surface and the truncated octahedral Au₃₈ cluster with respect to the RGL potential. In particular, it can be noted how: (a) the “rounding” of the (111) face in the Au(110) surface—both the simplified “surface-only” system and the complete system (note that the latter has not been used as a fitting system)—is now described in a qualitatively correct way (see the sign of Δy_2 in Table I), (b) the z -coordinate of the atoms lying on (111) faces of the Au₃₈ cluster are remarkably expanded, in agreement with the DF/PW91 results but at variance with the RGL results. The new potential thus seems to be able to describe the fitting systems also in a neighborhood of the ideal configurations which have been used in the fitting procedure.

As a further test of the new potential, the lowest-energy structures of small gold clusters (with size between 6 and 200 atoms) were investigated. Extracted from these calculations, the putative global minima of Au₁₄, Au₂₀, and Au₃₂ according to the new potential are shown in Fig. 8, together with the corresponding binding energies. These structures were obtained through basin-hopping runs comprising 1000 Monte Carlo steps starting from randomly chosen initial configurations and allowing random moves of up to 1 Å (positive or negative) in the Cartesian coordinates of each atom (a value of $kT=0.5$ eV was chosen). It is interesting to note that for Au₃₂ the proposed cage structure coincides with the highly symmetrical icosahedral structure proposed as the global minimum.⁴⁷ This does not hold for Au₂₀, for which the putative global minimum given by the potential is structurally different from the tetrahedral structure which is

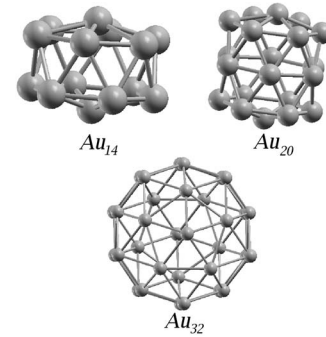


FIG. 8. Schematic representation of the putative global minima of Au₁₄ (2.823 eV/atom), Au₂₀ (3.007 eV/atom), and Au₃₂ (3.210 eV/atom).

thought to be the ground state in the gas phase.⁴⁸ However, shell closure effects have been shown to be essential in stabilizing the Au₂₀ tetrahedron with respect to cage structures¹⁶ and, of course, we cannot aim at describing effects, such as quantum (shell closure/unclosure, electronic wave function or magnetic interference) effects, which are by definition outside the scope of empirical potential approaches. In general, we found that small gold clusters have a great tendency toward cage configurations according to the new potential: we estimated that the transition from cage to compact (fcc-like) structures only occurs around size $N=150$ atoms. This tendency is probably overestimated with respect to DF/PW91 predictions.⁴⁹

VII. CONCLUSIONS

From a detailed analysis of DF/PW91 calculations on gold model clusters and surfaces, an empirical potential for gold, which includes angular corrections, has been derived in the present article. It consists in the inclusion of higher-order nonlinear terms (specifically, the product dipole-quadrupole) that do not appear to have been used before, but that our analysis suggests to be necessary to describe directionality effects in the Au-Au interaction. Preliminary tests show that this potential is able to describe in a reasonably accurate way the systems used in the fitting procedure also in a neighborhood of the ideal configurations thereby used, and that it possesses some unusual features with respect to existing potentials, such as a strong tendency toward cage structures for small Au clusters.¹⁶ It thus represents a good starting point for future investigations (currently in progress in our lab). In particular, we stress that even though the present formulation probably overestimates the tendency of gold to open structures, it is important to have a potential available which gives qualitatively different results with respect to the existing ones and can thus “bracket” the experimental behavior. This point should be particularly useful when using such potentials in combined empirical potential/first-principles systematic searches.⁵⁰ Another intriguing possibility is to use a weighted average (with weights to be optimized) of the new potential and, say, the RGL potential, which is known to favor in an excessive way compact structures.¹⁶

A final remark: even though we are reasonably confident to have singled out the main physical origin of the angular

corrections to the Au-Au potential, the present formulation is obviously not the only possible one, and the inclusion of a more extensive set of DF data is in order to further improve the accuracy of the proposed parametrization. Moreover, in the absence of really accurate and complete experimental data, we resorted to a parametrization based on DF/PW91 results (only properly rescaling lengths and energies to match the experimental bulk values of binding energy and lattice constant), so that the present potential obviously suffers from the limitations of the rescaled DF/PW91 approach.

ACKNOWLEDGMENTS

We thank Dr. Pietro Ballone (Belfast) for useful discussions. We acknowledge financial support from the Italian CNR for the program “(Supra-) Self-Assemblies of Transition Metal Nanoclusters” within the framework of the ESF EUROCORES SONS, and from the European Community Sixth Framework Project for the STREP Project “Growth and Supra-Organization of Transition and Noble Metal Nanoclusters” (Contract No. NMP-CT-2004-001594).

*Present address: LAAS-CNRS, Av. du Colonel Roche 7, 31077 Toulouse, France.

†Corresponding author. fortunelli@ipcf.cnr.it

¹V. Rosato, M. Guillopé, and B. Legrand, *Philos. Mag. A* **59**, 321 (1989).

²M. S. Daw and M. I. Baskes, *Phys. Rev. B* **29**, 6443 (1984).

³F. Ercolessi, M. Parrinello, and E. Tosatti, *Philos. Mag. A* **58**, 213 (1988).

⁴F. Ercolessi, E. Tosatti, and M. Parrinello, *Phys. Rev. Lett.* **57**, 719 (1986).

⁵A. Bartolini, F. Ercolessi, and E. Tosatti, *Phys. Rev. Lett.* **63**, 872 (1989).

⁶M. I. Baskes, *Phys. Rev. Lett.* **59**, 2666 (1987).

⁷M. I. Baskes, *Phys. Rev. B* **46**, 2727 (1992).

⁸M. I. Baskes, J. S. Nelson, and A. F. Wright, *Phys. Rev. B* **40**, 6085 (1989).

⁹M. I. Baskes and R. A. Johnson, *Modell. Simul. Mater. Sci. Eng.* **2**, 147 (1994).

¹⁰Y. Mishin, M. J. Mehl, and D. A. Papaconstantopoulos, *Acta Mater.* **53**, 4029 (2005).

¹¹B.-J. Lee, J.-H. Shim, and M. I. Baskes, *Phys. Rev. B* **68**, 144112 (2003).

¹²E. Aprà and A. Fortunelli, *J. Mol. Struct.: THEOCHEM* **501-502**, 251 (2000).

¹³A. Fortunelli and A. M. Velasco, *Int. J. Quantum Chem.* **99**, 654 (2004).

¹⁴E. Aprà, F. Baletto, R. Ferrando, and A. Fortunelli, *Phys. Rev. Lett.* **93**, 065502 (2004).

¹⁵R. Ferrando, A. Fortunelli, and G. Rossi, *Phys. Rev. B* **72**, 085449 (2005).

¹⁶E. Aprà, R. Ferrando, and A. Fortunelli, *Phys. Rev. B* **73**, 205414 (2006).

¹⁷P. Torelli, F. Sirotti, and P. Ballone, *Phys. Rev. B* **68**, 205413 (2003).

¹⁸P. Koskinen, H. Häkkinen, G. Seifert, S. Sanna, T. Frauenheim, and M. Moseler, *New J. Phys.* **8**, 1 (2006).

¹⁹D. G. Fedak and N. A. Gjostein, *Acta Metall.* **15**, 827 (1967).

²⁰D. Wolf, Ph.D. thesis, Universität München, Munich, 1972.

²¹W. Moritz and D. Wolf, *Surf. Sci.* **88**, L29 (1979).

²²D. Wolf, H. Jagodzinski, and W. Moritz, *Surf. Sci.* **77**, 265 (1978).

²³D. Wolf, H. Jagodzinski, and W. Moritz, *Surf. Sci.* **77**, 283 (1978).

²⁴Q. J. Gao and T. T. Tsong, *J. Vac. Sci. Technol. A* **15**, 761 (1987).

²⁵K. Müller, J. Witt, and O. Schütz, *J. Vac. Sci. Technol. A* **5**, 757 (1987).

²⁶G. L. Kellogg, *J. Vac. Sci. Technol. A* **5**, 747 (1987).

²⁷T. E. Jackman, J. A. Davies, D. P. Jackson, P. R. Norton, and W. N. Unertl, *Surf. Sci.* **120**, 389 (1982).

²⁸H. Niehus, *Surf. Sci.* **145**, 407 (1984).

²⁹J. Möller, K. J. Snowdon, W. Heiland, and H. Niehus, *Surf. Sci.* **176**, 475 (1986).

³⁰S. H. Overbury, W. Heiland, D. M. Zehner, S. Datz, and R. S. Thoe, *Surf. Sci.* **109**, 293 (1981).

³¹P. Häberle, P. Fenter, and T. Gustafsson, *Phys. Rev. B* **39**, 5810 (1989).

³²M. Copel, P. Fenter, and T. Gustafsson, *J. Vac. Sci. Technol. A* **5**, 742 (1987).

³³I. K. Robinson, *Phys. Rev. Lett.* **50**, 1145 (1983).

³⁴L. D. Marks, *Phys. Rev. Lett.* **51**, 1000 (1983).

³⁵G. Binnig, H. Rohrer, C. Gerber, and E. Weibel, *Surf. Sci.* **131**, L379 (1983).

³⁶S. Olivier, G. Tréglia, A. Saul, and F. Willaime, *Surf. Sci.* **600**, 5131 (2006).

³⁷S. Baroni, A. Dal Corso, S. de Gironcoli, and P. Giannozzi, PWSCF site <http://www.pwscf.org>

³⁸J. P. Perdew, J. A. Chevary, S. H. Vosko, K. A. Jackson, M. R. Pederson, D. J. Singh, and C. Fiolhais, *Phys. Rev. B* **46**, 6671 (1992).

³⁹V. Bonačić-Koutecky, J. Burda, R. Mitrič, M. Ge, G. Zampella, and P. Fantucci, *J. Chem. Phys.* **117**, 3120 (2002).

⁴⁰B. Soulé de Bas, M. J. Ford, and M. B. Cortie, *J. Mol. Struct.: THEOCHEM* **686**, 193 (2004).

⁴¹E. M. Fernández, J. M. Soler, I. L. Garzón, and L. C. Balbás, *Phys. Rev. B* **70**, 165403 (2004).

⁴²F. Remacle and E. S. Kryachko, *Advances in Quantum Chemistry* (Elsevier, Amsterdam, 2004).

⁴³F. Ercolessi and J. B. Adams, *Europhys. Lett.* **26**, 583 (1994).

⁴⁴X. Y. Liu, F. Ercolessi, and J. B. Adams, *Modell. Simul. Mater. Sci. Eng.* **12**, 665 (2004).

⁴⁵Z. Li and H. A. Scheraga, *Proc. Natl. Acad. Sci. U.S.A.* **84**, 6611 (1987).

⁴⁶D. J. Wales and J. P. K. Doye, *J. Phys. Chem. A* **101**, 5111 (1997).

⁴⁷M. P. Johansson, D. Sundholm, and J. Vaara, *Angew. Chem., Int. Ed.* **43**, 2678 (2004).

⁴⁸J. Li, X. Li, H.-J. Zhai, and L.-S. Wang, *Science* **299**, 864 (2003).

⁴⁹S. Bulusu, X. Li, L.-S. Wang, and X.-C. Zeng, *J. Phys. Chem. C* **111**, 4190 (2007).

⁵⁰R. Ferrando, A. Fortunelli, and R. L. Johnston, *Phys. Chem. Chem. Phys.* **10**, 640 (2008).